

Role of covalent and metallic intercalation on the electronic properties of epitaxial graphene on SiC(0001)

I. Deretzis* and A. La Magna

Istituto per la Microelettronica e Microsistemi (CNR-IMM), VIII strada 5, I-95121 Catania, Italy

(Dated: July 21, 2022)

We present an orbital-resolved density functional theory study on the electronic properties of hydrogen and lithium intercalated graphene grown on the Si-face of SiC. Starting from the $6\sqrt{3} \times 6\sqrt{3}R30^\circ$ surface reconstruction of the graphene/SiC heterosystem, we find that both H and Li can restore the ideal structural characteristics of the two nonequivalent junction parts (i.e. graphene and the SiC substrate) when inserted at the interface. However the chemical/electrostatic interactions remain different for the two cases. Hence, H-intercalated graphene is subject to a sublattice symmetry-breaking electronic interference that perturbs the Dirac point, whereas Li-intercalation gives rise to a highly n -doped system due to a non-uniform delocalization of Li charges.

PACS numbers: 81.05.ue, 73.22.Pr

Graphene is a single-atom-thick crystal of sp^2 -hybridized carbons that exhibits exceptional electronic properties due to its linear dispersion relation around the Dirac point¹. During the last years the quest for its use in fundamentals and applications has boosted the research on processes that could allow for a controlled synthesis of ordered graphene layers. Within this context, epitaxial growth on SiC substrates has emerged as one of the principal technologies for large-scale graphene fabrication^{2,3}. The process could be better described as a “de-growth” one since SiC crystals are heated up to temperatures that allow for an extremely higher sublimation rate of the Si atoms with respect to the C ones. These remaining C surface atoms recombine to form thin graphite films. A proper calibration of the process parameters⁴ can allow for the formation of single graphene layers directly grown on a semi-insulating substrate, i.e. with no need to be transferred elsewhere after the end of the thermal treatment.

Epitaxial graphene can grow on both the Si and C faces of the (0001) surface of hexagonal SiC polytypes⁵, or similarly at the (111) surface of cubic SiC⁶. Even if both theory^{7,8} and experiment⁹ argue that C-face epitaxial graphene should electrically suffer less interferences from the substrate, Si-face growth results slower⁴ and hence a better control can be achieved on the formation of single or few-layer structures. In this case a first carbon-rich interface layer with a $6\sqrt{3} \times 6\sqrt{3}R30^\circ$ surface reconstruction strongly binds to the substrate and is the precursor of the overlying graphene films^{5,10}. Experimental evidence shows that the presence of this carbon layer has a negative influence in the conduction properties of the heterosystem with respect to the SiO_2 -deposited case, in terms of enhanced surface polar phonon scattering¹¹, reduced mean-free paths¹¹ and temperature-dependent mobilities¹², which are characteristic of the diffusive transport regime. To this end, intercalation techniques with various elements have been proposed in the literature^{13–16} in order to detach this layer from the substrate and minimize the interface interaction.

In this article we study the structural and electronic properties of H and Li-intercalated epitaxial graphene within a comparative approach of functionalization with adatoms that interact in a covalent and a metallic way with the substrate. As a starting point we recognize the problems related to the presence of the strongly-bound carbon-rich layer within a density functional theory (DFT) description of the $6\sqrt{3} \times 6\sqrt{3}R30^\circ$ reconstruction. We then proceed with an analysis of the structural and electronic symmetry of the intercalated systems, arguing that the resulting chemically modified interfaces are different in terms of effective doping, bonding and electrostatic interactions. Results bring to discussion the versatility of substrate engineering in tailoring the physical properties of epitaxial graphene on SiC.

We use the DFT SIESTA computational code¹⁷ to perform *ab initio* calculations treating electronic correlations within the local density approximation (LDA)¹⁸, which has been shown to describe properly the experimental aspects of the graphene/SiC interface¹⁰. Moreover, taking into account the absence of nonlocal dispersive interactions in the LDA, we also perform a comparative analysis for the intercalated systems using different exchange-correlation functionals: in the spirit of Ref. 19, apart from the LDA we use the Perdew-Burke-Ernzerhof implementation²⁰ of the generalized gradient approximation (GGA) and the van der Waals (VDW) functional of Dion *et al*^{21,22}. The epitaxial graphene structures comprise of two bilayers of a $6\sqrt{3} \times 6\sqrt{3}R30^\circ$ SiC substrate (passivated with H at the bottom) over which a single 13×13 graphene supercell relaxes in order to satisfy lattice commensuration. The aspect of the correct surface reconstruction is fundamental in the computational modeling of the designed system. Indeed, models based on the simpler $\sqrt{3} \times \sqrt{3}R30^\circ$ reconstruction^{23–25}, although efficient in describing some of the basic electronic properties of the SiC/graphene interface (e.g. n -type doping and presence of the carbon-rich layer), are characterized by: (a) the absence of commensuration for the graphene and the SiC lattices that leads to an 8% stretching of the graphene sheet, and (b) a small graphene supercell.

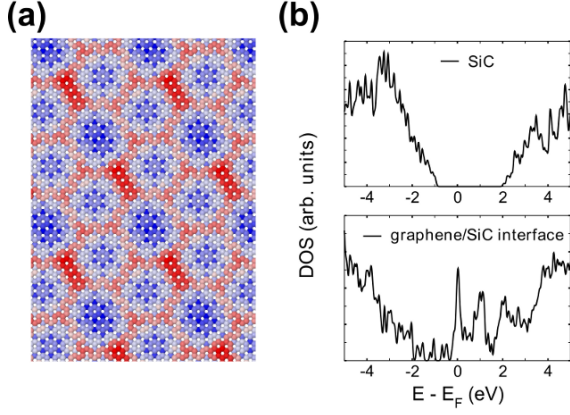


FIG. 1. (a) Color map topmost view of the $6\sqrt{3} \times 6\sqrt{3}R30^\circ$ -reconstructed first carbon-rich layer of an epitaxial graphene system showing the vertical positions of the C atoms, where a gradual red to blue coloring indicates bigger to smaller distances from the substrate. (b) Density of states as a function of energy for an ideal 4H-SiC crystal (upper) and the graphene/SiC(0001) interface (lower).

Repercussions of these aspects with respect to the results obtained by the actual $6\sqrt{3} \times 6\sqrt{3}R30^\circ$ surface symmetry are discussed in the following.

We model three different systems, i.e. the graphene/SiC interface before and after intercalation with H and Li, considering a full and uniform coverage of the substrate by the intercalating element in the form of a monolayer. A basis set of double- ζ Sankey-type valence orbitals has been used for C, Si and H, while polarization orbitals have been added in the case of Li. Convergence tests on a $\sqrt{3} \times \sqrt{3}R30^\circ$ -based system have shown that the previous set can reproduce the main band structure features obtained by a more accurate basis. We exploit the localized character of the atomic orbitals in order to calculate the single-orbital contributions in the composite electronic band structure: for each nonequivalent k -point sampled along the closed $\Gamma \rightarrow M \rightarrow K \rightarrow \Gamma$ Brillouin-zone path we calculate the wave functions $\Psi_{n,\mathbf{k}}$ corresponding to the n eigenstates. Based on the linear combination of atomic orbitals $\Psi_{n,\mathbf{k}} = \sum_i c_i \phi_i$ (where c_i are the weighting coefficients and ϕ_i the atomic orbitals) we calculate the square modulus of the total weight of the single orbitals at the n^{th} eigenstate as: $w_t = \sum_j |c_j|^2$, where the integration runs over those indices $j \leq i$ for which we want to calculate the contributions in the electronic structure. Contrary to the variational approach in the calculation of the valence electronic properties, the electronic contribution of the ionic cores is statically described with norm-conserving Troulier-Martins pseudopotentials²⁶ that have been tested to accurately reproduce the band structure of hexagonal SiC polytypes and graphene. The minimization of the electron density is achieved by sampling the Brillouin zone with a single-point Monkhorst-Pack grid for the $6\sqrt{3} \times 6\sqrt{3}R30^\circ$ model and a $7 \times 7 \times 1$ grid for the $\sqrt{3} \times \sqrt{3}R30^\circ$ one. A mesh

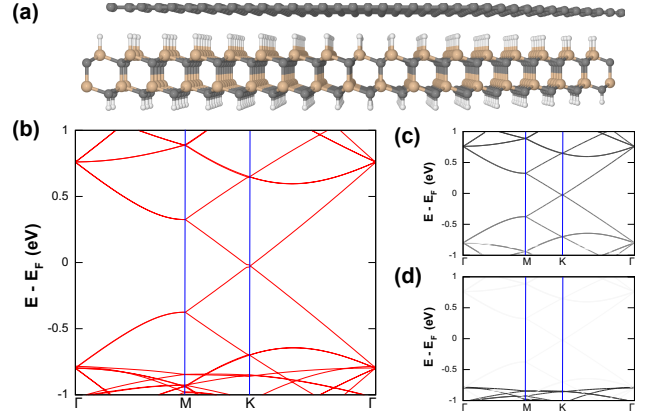


FIG. 2. (a) Geometry of the relaxed H-intercalated epitaxial graphene system. (b) Total band structure of the H-intercalated system. (c) Contributions of the $2p_z$ orbitals of the graphene layer in the total band structure. (d) Contributions of the substrate orbitals in the total band structure.

cutoff energy of 350 *Ryd* has been imposed for real-space integration, while all structures have been relaxed with a force criterion of 0.06 eV/Å.

As a first step towards understanding the need for intercalation in epitaxial graphene systems grown on the Si-face of SiC we calculate the structural and electronic properties of the $6\sqrt{3} \times 6\sqrt{3}R30^\circ$ graphene/SiC interface. The relaxation of the corresponding supercell gives rise to a corrugated carbon layer with a thickness of ~ 1.5 Å. The surface is characterized by height-varying Moiré patterns that form hexagons with edges of 10-12 Å, which correspond to the regions of the carbon layer that are more distant from the substrate (see the red areas in Fig. 1(a)). This structural deformation with respect to the ideal lattice topology is also reflected in terms of the chemical bonding, where an interplay between sp^2 and sp^3 interface interactions appears, with a strong preferential disposition towards the sp^3 scheme, in contrast with the respective interface of C-face epitaxial graphene⁸. This aspect reflects the weakness of the π -bond in Si with respect to C. The electronic properties of the heterosystem (Fig. 1(b)-lower) are characterized by: (a) a peak in the density of states at the Fermi level (E_F) of the system that originates from the sp^2 -hybridized Si atoms of the interface. (b) The presence of surface states throughout the bulk substrate's band-gap, with a prevalent contribution from the $2p_z$ orbitals of the carbon epilayer. This last feature is not captured by simpler $\sqrt{3} \times \sqrt{3}R30^\circ$ model and could be related to the manifestation of leakage interface currents during conduction.

Si-face grown epitaxial graphene can be used as a reference system for the study of a number of fundamental physical properties²⁷ without the need of further processing. However, the electrical use of such a material within a device concept dictates the need of interface passivation with functional adatoms through a post-growth chemical

model	LDA	GGA	VDW
$\sqrt{3} \times \sqrt{3}R30^\circ$	130 meV	80 meV	15 meV
$6\sqrt{3} \times 6\sqrt{3}R30^\circ$	8 meV	5 meV	5 meV

TABLE I. Comparison of the energy gap values (E_g) of the H-intercalated epitaxial graphene system for the $\sqrt{3} \times \sqrt{3}R30^\circ$ and the $6\sqrt{3} \times 6\sqrt{3}R30^\circ$ models within the LDA, GGA and VDW exchange-correlation functionals.

process. The simplest example of intercalation from a monovalent element is that of hydrogen, as proposed by Riedl *et al.*¹³ and followed by others^{12,28}. Starting from the $6\sqrt{3} \times 6\sqrt{3}R30^\circ$ reconstruction of the carbon-rich layer we model H-intercalation by assigning a single H atom on top of each Si atom of the substrate's surface, as confirmed by infrared absorption spectroscopy¹². Upon relaxation, H atoms covalently bind with the interface Si atoms and restore the ideal sp^3 hybridization of the substrate (Fig. 2(a)). As a result, the structurally disordered carbon layer turns into an almost detached flat graphene sheet with a distance of 2.39 Å from the H-interface layer and 3.92 Å from the substrate Si atoms. The electronic band structure of this system shows the 13×13 folded graphene bands and confirms the minimal interaction with the substrate (Fig. 2(b)). However a small perturbation appears at the Dirac point that opens a bandgap of few millielectronvolts, in analogy with a similar feature calculated for the interaction between graphene and the (0001) surface of SiO_2 ²⁹. We find this perturbation robust for small horizontal shifts of the graphene layer with respect to the substrate. Even if this gap is extremely small, well beyond $k_B T$ at room temperature and difficult to reveal in experiments, its physical origin is of a particular interest. A careful analysis of the electronic Hamiltonian of the composite system excludes an intra-valley contribution on the electronic perturbation. Instead, the origin of this interference can be traced at the breaking of the sublattice symmetry³⁰ due to the unequal coupling between the two interpenetrating triangular lattices of the graphene sheet and the localized Si-H dipoles of the substrate, which have non-equivalent positions with respect to the graphene atoms in the supercell. For the smaller $\sqrt{3} \times \sqrt{3}R30^\circ$ model, this symmetry-breaking effect acquires an extreme form due to the fact that the graphene sheet is defined by only eight periodically reproduced C atoms and manifests in the form of wider band gaps in the electronic band structure (see Table I). In this case, the choice of the exchange-correlation functional becomes critical and both the LDA and the GGA overestimate the graphene-substrate interaction. However, when considering the $6\sqrt{3} \times 6\sqrt{3}R30^\circ$ model with 338 graphene atoms in the supercell, the sublattice differences get averaged out and all functionals converge in a minor band gap. A second issue worth mentioning for the $\sqrt{3} \times \sqrt{3}R30^\circ$ case is the shift of the graphene eigenstates with respect to the substrate levels due to fictitious strain, which results in a positioning of the Dirac

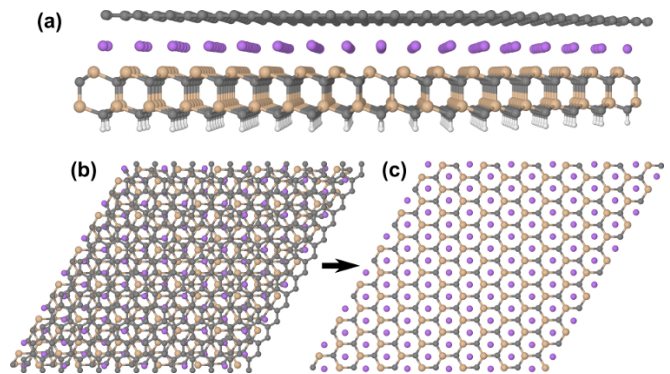


FIG. 3. (a) Side view of the relaxed Li-intercalated epitaxial graphene system. (b) Top view of the Li-intercalated system. (c) Top view showing only the Li atoms that occupy the hollow positions of the first SiC bilayer.

cone closer to the valence band of SiC with respect to the bigger supercell. Nonetheless, all models converge in the designation of charge neutrality at the Dirac point.

The main problem with the use of atomic hydrogen in the chemical detachment of the graphene/SiC interface is that it can also functionalize the graphene layer itself³¹, giving rise to sp^3 -type defects. A possible solution towards this direction could be the intercalation with elements that do not disturb the planarity and the sp^2 character of the graphene sheet. Lithium fulfills this prerequisite³². Experimentally Li-intercalation has been proposed by Virojanadara *et al.*¹⁴ who showed that Li, as a highly reactive lightweight monovalent metal, can penetrate the strongly-bound carbon-rich layer and position on top of the SiC substrate. Stimulated by such experiment, we model Li-intercalated epitaxial graphene systems considering an equivalent to H complete coverage of the SiC surface. Structurally, also in this case the carbon interface layer relaxes into a flat graphene sheet with a vertical distance of 2.37 Å from the Li-adlayer and 4.41 Å from the Si atoms of the substrate (Fig. 3(a)). However, as a first difference with respect to the H case, we find that the minimum-energy configuration for the relaxation of Li atoms is at the hollow positions of the first substrate bilayer (Fig. 3(b-c)). The reason of this symmetry originates from the bonding interactions between the Li adlayer and the substrate. We find an important charge transfer from the Li atoms to a region between Li and the Si atoms of the substrate's surface, localized on the top of the Si atomic positions. Such configuration guarantees the pure sp^3 hybridization of the substrate, leaving a cation at the location of the Li atom. The unequal chemisorption of H and Li on the graphene/SiC interface could be also reflected in a different sub-graphene inter-diffusion mechanism during the intercalation process.

The electronic band structure obtained by this composite system shows highly-concentrated bands throughout the hole region of the spectrum that are difficult to interpret. In this sense an orbital-resolved analysis is nec-

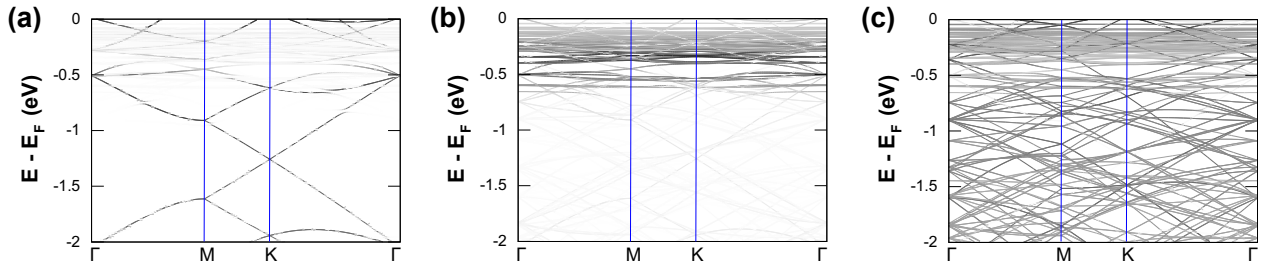


FIG. 4. Orbital-resolved band structure for the Li-intercalated epitaxial graphene system, showing the contributions of the (a) $2p_z$ orbitals originating from the graphene C atoms, (b) all orbitals originating from Li atoms and (c) all orbitals originating from the substrate C/Si atoms.

essary for the determination of the local contributions in the total electronic structure. Considering therefore the contribution of the $2p_z$ orbitals coming from the graphene layer, we obtain a band structure that is equal to that of ideal graphene for a large energy range around the Dirac point (Fig. 4(a)). This result denotes that the detachment from the substrate also in the case of Li intercalation is almost complete, while unlike the H-intercalated case we do not obtain any interference at the Dirac point due to a better screening of the substrate from the Li ionic cores. The important aspect though is that the graphene sheet is highly electron-doped (as also calculated for a low-coverage Au intercalation³³), with the Dirac cone lying $\sim 1.3\text{eV}$ below the Fermi level of the heterosystem. This high effective doping is due to the electrostatic interactions between the graphene layer and the Li cations, which gives rise to a shift of the graphene bands within the valence band region of the SiC substrate (Fig. 4(c)), making the whole system electrically active at the vicinity of the Dirac point. The analysis of the electronic Hamiltonian of the composite system here shows an important decrease of the on-site energies of the C atoms with respect to the case of H-intercalation. This aspect is important if we consider that the actual intercalation process may not be uniform throughout the entire breadth of the graphene layer. In this case we can expect an Anderson-type disorder arising from the energetic mismatch between intercalated and non-intercalated regions. A further difference between the H and Li-intercalated systems results from the calculation of the binding energies of the graphene atoms, where the LDA values are 60

meV and 108 meV per C atom respectively. Finally, it is interesting to note that the quasi-flat bands originating from the Li orbitals (Fig. 4(b)) maintain a higher-energy position with respect to the Dirac cone.

To conclude, in this article we have studied within a DFT framework the electronic structure properties of the non-intercalated as well as the H/Li-intercalated interfaces between graphene and the Si-face of SiC, starting from the actual $6\sqrt{3} \times 6\sqrt{3}R30^\circ$ reconstruction of the graphene/SiC interface. We identified some issues related to the graphene/SiC coupling like the presence of midgap interface states throughout the SiC bandgap that could be related to plausible faults in the expected electrical behavior. We thereon studied two different intercalated systems with H and Li adatoms and saw that although in both systems the strongly-bound carbon-rich layer is detached from the substrate, different electronic properties distinguish the two cases: in the case of H-intercalation we observed a minimal perturbation at the Dirac point as a consequence of substrate-induced interference from localized Si-H dipoles, while in the case of Li-intercalation we obtained a highly n -doped ideal graphene bandstructure with the position of the Dirac cone within the valence band of the SiC substrate. A critical comparison between these two examples unfolds the potentiality of substrate engineering in epitaxial graphene structures.

This work has been partially supported by the European Science Foundation (ESF) under the EUROCORES Program EuroGRAPHENE CRP GRAPHIC-RF. Computations have been performed at the CINECA supercomputing facilities under project TRAGRAPH.

* ioannis.deretzis@imm.cnr.it

¹ A. H. Castro Neto *et al.*, Rev. Mod. Phys. **81**, 109 (2009).
² K. V. Emtsev *et al.*, Nature Materials **8**, 203 (2009).
³ C. Dimitrakopoulos *et al.*, J. Vac. Sci. Technol. B **28**, 985 (2010).
⁴ G. G. Jernigan *et al.*, Nano Letters **9**, 2605 (2009).
⁵ J. Hass, W. A. de Heer, and E. H. Conrad, Journal of Physics Condensed Matter **20**, F3202+ (2008).
⁶ A. Ouerghi *et al.*, Appl. Phys. Lett. **96**, 191910 (2010).
⁷ O. Pankratov, S. Hensel, and M. Bockstedte, Phys. Rev.

B **82**, 121416 (2010).

⁸ I. Deretzis and A. La Magna, Appl. Phys. Lett. **98**, 023113 (2011).
⁹ X. Wu *et al.*, Appl. Phys. Lett. **95**, 223108 (2009).
¹⁰ S. Kim *et al.*, Phys. Rev. Lett. **100**, 176802 (2008).
¹¹ S. Sonde *et al.*, Appl. Phys. Lett. **97**, 132101 (2010).
¹² F. Speck *et al.*, ArXiv e-prints (2011), arXiv:1103.3997.
¹³ C. Riedl *et al.*, Phys. Rev. Lett. **103**, 246804 (2009).
¹⁴ C. Virojanadara *et al.*, Phys. Rev. B **82**, 205402 (2010).
¹⁵ A. L. Walter *et al.*, Appl. Phys. Lett. **98**, 184102 (2011).

- ¹⁶ I. Gierz *et al.*, Phys. Rev. B **81**, 235408 (2010).
- ¹⁷ J. M. Soler *et al.*, Journal of Physics Condensed Matter **14**, 2745 (2002).
- ¹⁸ J. P. Perdew and A. Zunger, Phys. Rev. B **23**, 5048 (1981).
- ¹⁹ T. Jayasekera, S. Xu, K. W. Kim, and M. B. Nardelli, Phys. Rev. B **84**, 035442 (2011).
- ²⁰ J. P. Perdew, K. Burke, and M. Ernzerhof, Phys. Rev. Lett. **77**, 3865 (1996).
- ²¹ M. Dion, H. Rydberg, E. Schröder, D. C. Langreth, and B. I. Lundqvist, Phys. Rev. Lett. **92**, 246401 (2004).
- ²² G. Román-Pérez and J. M. Soler, Phys. Rev. Lett. **103**, 096102 (2009).
- ²³ I. Deretzis and A. La Magna, Appl. Phys. Lett. **95**, 063111 (2009).
- ²⁴ A. Mattausch and O. Pankratov, Phys. Rev. Lett. **99**, 076802 (2007).
- ²⁵ F. Varchon *et al.*, Phys. Rev. Lett. **99**, 126805 (2007).
- ²⁶ N. Troullier and J. L. Martins, Phys. Rev. B **43**, 1993 (1991).
- ²⁷ A. Tzalenchuk *et al.*, Nature Nanotechnology **5**, 186 (2010).
- ²⁸ C. Virojanadara *et al.*, Surface Science **604**, L4 (2010).
- ²⁹ N. T. Cuong, M. Otani, and S. Okada, Phys. Rev. Lett. **106**, 106801 (2011).
- ³⁰ S. Y. Zhou *et al.*, Nature Materials **6**, 770 (2007).
- ³¹ S. Casolo *et al.*, J. Chem. Phys. **130**, 054704 (2009).
- ³² M. Khantha *et al.*, Phys. Rev. B **70**, 125422 (2004).
- ³³ F.-C. Chuang *et al.*, Nanotechnology **22**, 275704 (2011).